European Polymer Journal 116 (2019) 361–369

Contents lists available at ScienceDirect

European Polymer Journal

journal homepage: www.elsevier.com/locate/europolj

Hydrogen bonding induces unusual self-assembled structures from mixtures of two miscible disordered diblock copolymers

Tzu-Chun Tseng[a], Shiao-Wei Kuo[a,b]

[a] Department of Materials and Optoelectronic Science, Center of Crystal Research, National Sun Yat-Sen University, Kaohsiung 80424, Taiwan
[b] Department of Medicinal and Applied Chemistry, Kaohsiung Medical University, Kaohsiung, Taiwan

ARTICLE INFO

Keywords:
Miscible disorder diblock copolymer
Hydrogen bonding strength
Self-assembly structure
Dipole-dipole interaction

ABSTRACT

We synthesized two miscible disordered diblock copolymers, poly(methyl methacrylate–*b*–vinylphenol) (PMMA-*b*-PVPh) and poly(4-vinylpyridine–*b*–ethylene oxide) (P4VP-*b*-PEO), through anionic living and reversible addition fragmentation chain transfer polymerizations, respectively; together, these polymers contained one hydrogen bond donor (PVPh) and three hydrogen bond acceptors (P4VP, PEO, PMMA). The inter-association equilibrium constants (K_A) for the three different hydrogen bonded pairs followed the order PVPh/P4VP (K_A = 1200) > PVPh/PEO (K_A = 280) > PVPh/PMMA (K_A = 47.1), suggesting that the PVPh units prefer to hydrogen bond with P4VP block, rather than PEO and PMMA blocks. Nevertheless, the excluded PMMA and PEO segments experienced weak intermolecular dipole–dipole interactions, such that the PMMA-*b*-PVPh/P4VP-*b*-PEO blends exhibited two-phase behavior, forming miscible PVPh/P4VP and PMMA/PEO phases, as evidenced using transmission electron microscopy.

1. Introduction

Polymer blends often possess superior thermal, mechanical, and optoelectronic properties when compared with those of their individual polymers [1–5]. In general, two types of phase structures are observed: immiscible blends that lack specific interactions [Scheme 1(A)-(a); two single-phase systems that undergo macrophase separation] and miscible blends that feature specific interactions [Scheme 1(A)-(b); two single phases that form a miscible disordered structure]. Simple homopolymer/homopolymer blend systems usually do not form self-assembled nanostructures exhibiting microphase separation. A blend system comprising linear homopolymers functionalized at their chain ends with multiple hydrogen bonding motifs or metal-ligand interactions could form the self-assembly nanostructure displayed in Scheme 1(B), a so-called supramolecular diblock copolymer (the two single phases transform to a two-phase structure with microphase separation) [6–10].

Self-assembled structures are usually induced from immiscible diblock copolymers (A-*b*-B), which typically form long-range-ordered lamellar, cylinder, spherical, and double-gyroid structures, with potential applications in photonic crystals, drug delivery, and nanolithography [11–17]. Blending with a homopolymer C or another diblock copolymer C-*b*-D can be used, with specific interactions (e.g., hydrogen bonding), to vary the volume fraction of each block segment and, thus, prepare well-defined nanostructures [18–39]. In general, two different types of microphase separation occur for the diblock copolymers in A-*b*-B/C blend, leading to two-phase system [Scheme 2(A)], depending on the miscibility of the segments of the diblock copolymer. The first type of microphase separation—which is depicted in Scheme 2(a) as a two-phase and a single-phase forming a two-phase system—has been observed from blends of immiscible PS-*b*-PVPh with P2VP, P4VP, and PMMA homopolymers; from PS-*b*-P2VP/PVPh blends; and from blends of P4VP-*b*-PCL or P2VP-*b*-PCL with phenoxy, PVPh and phenolic homopolymers [20–32]. The second type of microphase separation—in Scheme 2(b), two single-phase systems forming a two-phase system—has been found from the unusual miscible diblock copolymers PMMA-*b*-PVPh or PCL-*b*-PVPh blended with PVP homopolymers, mediated by the strength of the hydrogen bonding [33–36].

For A-*b*-B/C-*b*-D mixtures, systems in which intermolecular hydrogen bonding exists between B and C block segments, while A and D blocks are immiscible, can form the hierarchical self-assembled structures, including three-phase lamellae or core–shell cylinders [Scheme 2(c): two two-phase systems form a three-phase system] [40–49]. For example, Matsushita et al. reported that PS-*b*-PVPh blending with P2VP-*b*-PI induced hierarchical self-assembled structures such as cylinder-within-lamellar or simple lamellar-within-lamellar structures [42]. We have also previously noted three-phase behavior, both in solid state and solution, from PS-*b*-PVPh blended with P4VP-*b*-

E-mail address: kuosw@faculty.nsysu.eu.tw (S.-W. Kuo).

https://doi.org/10.1016/j.eurpolymj.2019.04.037
Received 23 January 2019; Received in revised form 8 April 2019; Accepted 17 April 2019
Available online 19 April 2019
0014-3057/

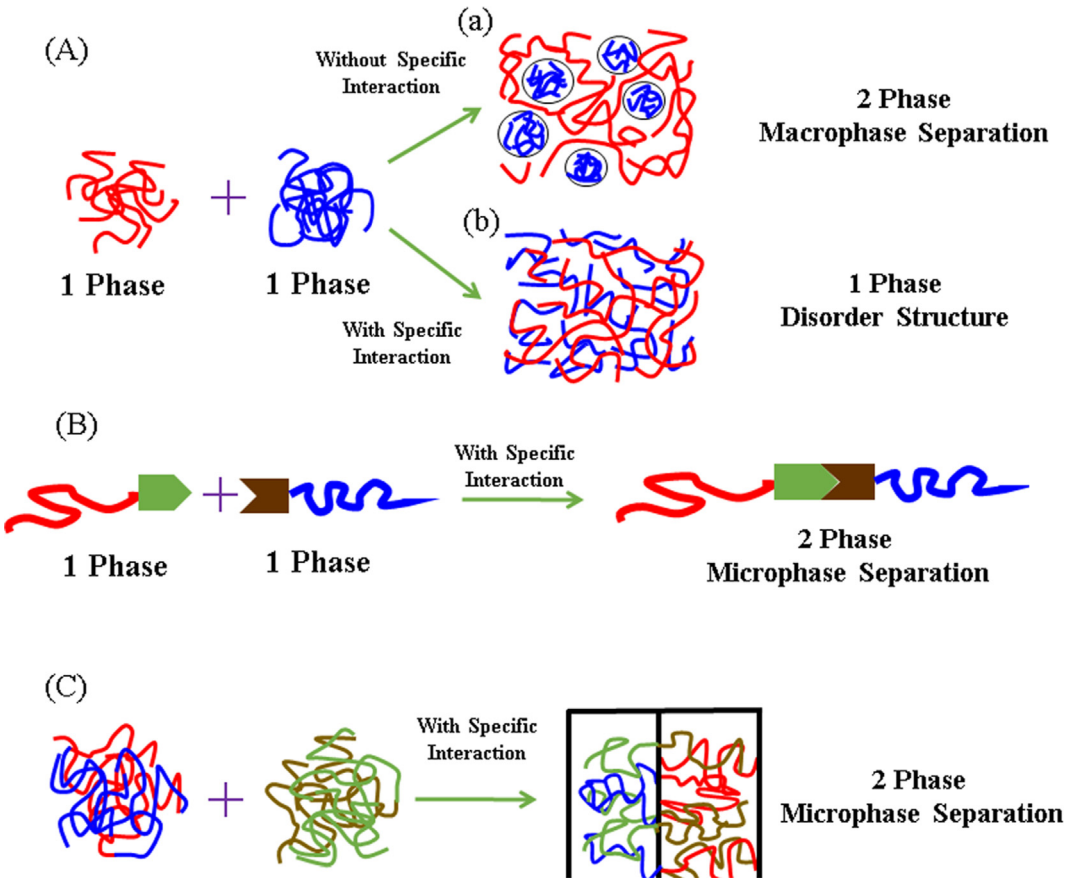

Scheme 1. Cartoon representations of pairs of single-phase systems (A) A + B becoming (a) a two-phase system (macrophase separation without specific interactions) and (b) a single-phase system (miscible disordered structure with specific interactions), (B) A + B becoming a two-phase system (microphase separation with strong chain-end-specific interactions), and (C) A-*b*-B + C-*b*-D becoming a two-phase system (microphase separation with side-chain-specific interactions).

PMMA or P4VP-*b*-PCL [45–48]. Recently, we observed that immiscible A-*b*-B and miscible disordered C-*b*-D could also form the hierarchical self-assembled structures [Scheme 2(d): a two-phase and a single-phase forming a three-phase system], from PS-*b*-P4VP/PMMA-*b*-PVPh [50] and PS-*b*-PVPh/P4VP-*b*-PEO [51] blends.

In this present study we firstly proposed that two miscible disordered diblock copolymers—namely PMMA-*b*-PVPh and P4VP-*b*-PEO—could also form a self-assembled nanostructure, with the two single-phase structures forming a two-phase structure when blended [Scheme 1(C)]. This system is more complicated than the chain end-functionalized multiple hydrogen bondings linear homopolymer blends [Scheme 1(B)] and miscible diblock copolymer/homopolymer blends [Scheme 2(b)] that also transform two single-phase systems into two-phase systems, because this type of microphase separation involves four block segments in a diblock copolymer mixture. Herein, we report the competitive hydrogen bonding, miscibility, and self-assembled nanostructures formed from the PMMA-*b*-PVPh/P4VP-*b*-PEO blend.

2. Experimental section

2.1. Materials

Methyl methacrylate (Aldrich, 99%), 4-vinylpyridine (4VP, 95%, Acros), and 4-*tert*-butoxystyrene (tBOS, Aldrich, 99%) were distilled from CaH_2. Poly(ethylene glycol) 4-cyano-4-(phenylcarbonothioylthio) pentanoate (M_n = 10,000 g/mol) was purchased from Aldrich. The $PVPh_{137}$-*b*-$PMMA_{135}$ diblock copolymer (PDI = 1.10) was synthesized through anionic living polymerization of MMA and tBOS monomers, with subsequent hydrolysis, as shown in Scheme 3(a) and described previously [52]. The PEO_{220}-*b*-$P4VP_{82}$ diblock copolymer (PDI = 1.11) was prepared through RAFT polymerization [Scheme 3(b)], using a previously reported method [51]. Table 1 summarizes the molecular weights and thermal properties of these two diblock copolymers.

2.2. PMMA-b-PVPh/P4VP-b-PEO diblock copolymer blends

Mixtures of the diblock copolymers PMMA-*b*-PVPh and P4VP-*b*-PEO were prepared by using solution blending. Each diblock copolymer was dissolved separately in DMF, the common solvent for these four block segments. The individual solutions were mixed and then stirred for 48 h at room temperature; they were then placed in Teflon dishes and the DMF solvent was allowed to evaporate slowly at 80 °C for 48 h; finally, the diblock copolymer mixtures were dried at 130 °C under vacuum for 1 week to remove any residual solvent.

2.3. Characterization

Glass transition and melting temperatures were measured by the TA Q-20 instrument operated from –80 to + 280 °C (heating rate: 20 °C min^{-1}). Fourier transform infrared (FTIR) spectra of blend samples were determined using the Bruker Tensor 27 FTIR spectrophotometer and the KBr disk method; 32 scans were recorded with a resolution of 4 cm^{-1}. Small-angle X-ray scattering (SAXS) was measured by the BL23A1 beamline at the National Synchrotron Radiation Research Center (NSRRC), Taiwan (λ = 1.12 Å); the diblock copolymer mixtures were sealed between Kapton windows and measured at room temperature. Transmission electron microscopy (TEM) was performed using a JEOL 2100 microscope operated at 200 kV; the blend samples were cut into the ultrathin section (Leica ultra-cut microtome, diamond knife) and stained with I_2 to display the P4VP domains; accordingly, the

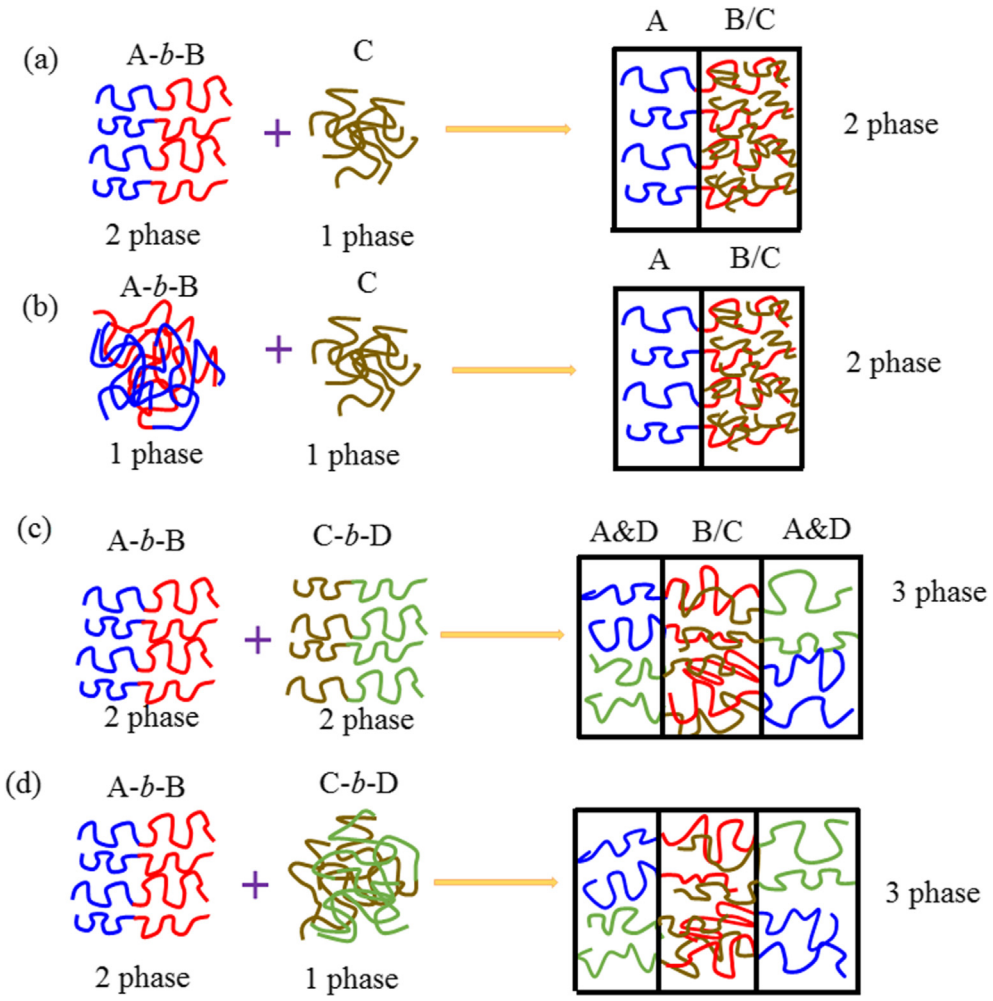

Scheme 2. Cartoon representations of the transformations of system experiencing specific interactions: (a) A-*b*-C + B becoming a two-phase system (2 phases + 1 phase becoming 2 phases), (b) A-*b*-B + C becoming a two-phase system (1 phase + 1 phase becoming 2 phases), (c) A-*b*-B + C-*b*-D becoming a three-phase system (2 phases + 2 phases becoming 3 phases), and (d) A-*b*-B + C-*b*-D becoming a three-phase system (2 phases + 1 phases becoming 3 phases).

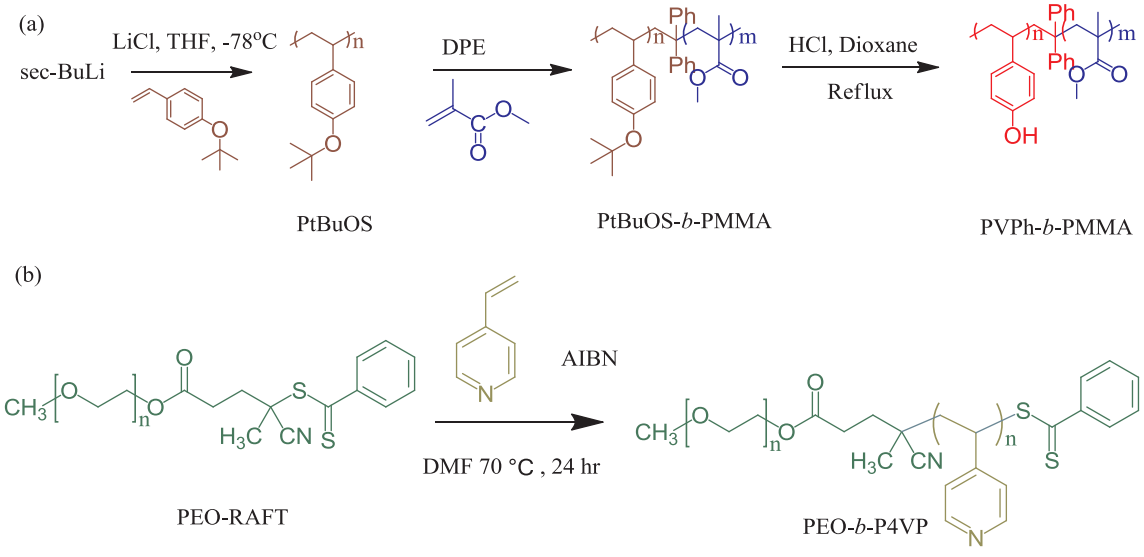

Scheme 3. Syntheses of (a) PMMA-*b*-PVPh through anionic polymerization and (b) P4VP-*b*-PEO through RAFT polymerization.

Table 1
Molecular weights and thermal properties of the PMMA-*b*-PVPh and of P4VP-*b*-PEO diblock copolymers synthesized in this study.

Block Copolymer	M_n (g/mol)	M_w/M_n	T_g/T_m(°C)
$PVPh_{137}$-*b*-$PMMA_{135}$	30,000[a]	1.10[a]	168/–
PEO_{220}-*b*-$P4VP_{82}$	18,610[b]	1.11[a]	140/61

[a] Obtained from GPC analysis by using PS as standard.
[b] Obtained by using ^{1}H NMR spectrum.

Table 2
Thermodynamic properties of the various different block segments used in this study.

Polymer	Molar Volume (mL/mol)	Molecular Weight (g/mol)	Solubility Parameter [(cal/mL)$^{1/2}$]	Equilibrium Constants		
				K_2	K_B	K_A
PVPh	82.3	120.1	11.0	21.0[a]	66.8[a]	
PMMA	84.9	100.0	9.1	–	–	47.1[b]
PEO	38.1	44.1	9.40	–	–	280[a]
P4VP	84.9	105.1	10.8	–	–	1200[a]

Self-association dimer (K_2) and multimer (K_B), and inter-association (K_A) equilibrium constants.
[a] Ref. [54].
[b] Ref. [52].

PVPh/P4VP domain appeared dark and the PMMA/PEO domain appeared white in TEM images.

3. Results and discussion

3.1. DSC and FTIR spectroscopic analyses of PMMA-b-PVPh/P4VP-b-PEO blends

We prepared the diblock copolymers PMMA-*b*-PVPh and P4VP-*b*-PEO, together featuring one hydrogen bond donor block and three hydrogen bond acceptor blocks, through anionic living and RAFT polymerizations, respectively (Scheme 3). Table 2 and Scheme 4 summarize the inter-association equilibrium constants for the PVPh block interacting with the P4VP, PEO, and PMMA block segments, as well as the molecular volume, solubility parameter, and molecular weight of each block segment. Six different interaction parameters would be expected for such PMMA-*b*-PVPh/P4VP-*b*-PEO blends (Scheme 4); five of them were negative, indicating that the PVPh/PMMA, PVPh/P4VP, PVPh/PEO, P4VP/PEO, and PEO/PMMA blend systems have disordered structures; the other was positive: that for the immiscible or phase-separated P4VP/PMMA binary blend system. The value of K_A of PVPh/P4VP blend (K_A = 1200) [53,54] was, however, much higher than the PVPh/PEO blend (K_A = 280) [54] or PVPh/PMMA in the diblock copolymer segment (K_A = 47.1) [52], suggesting that the PVPh segment prefers to hydrogen bond with the P4VP block, rather than with PEO and PMMA blocks. Therefore, although we might expect the PMMA and PEO blocks to be excluded from the miscible phase of blended PMMA-*b*-PVPh and P4VP-*b*-PEO diblock copolymers, the PMMA and PEO segments themselves feature a weak intermolecular dipole–dipole interaction and display miscible behavior [55–57]; accordingly, the PMMA-*b*-PVPh/P4VP-*b*-PEO blends did, indeed, exhibit two-phase behavior, forming miscible PVPh/P4VP and PMMA/PEO phases.

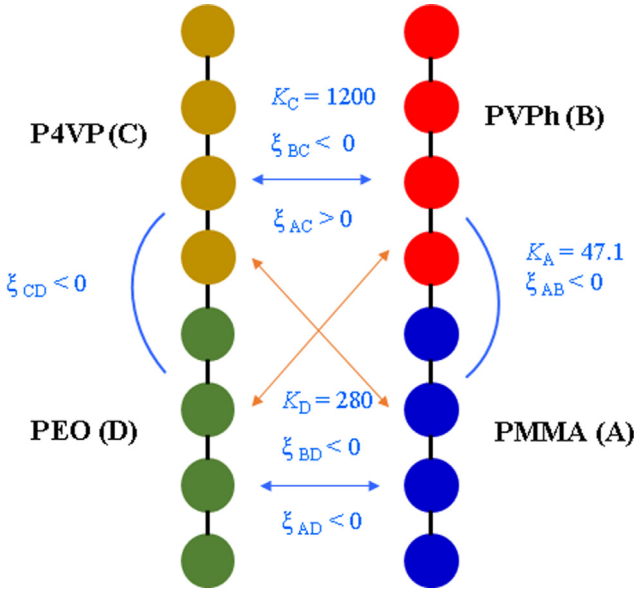

Scheme 4. Values of K_A and interaction parameters for PMMA-*b*-PVPh/P4VP-*b*-PEO diblock copolymer mixtures.

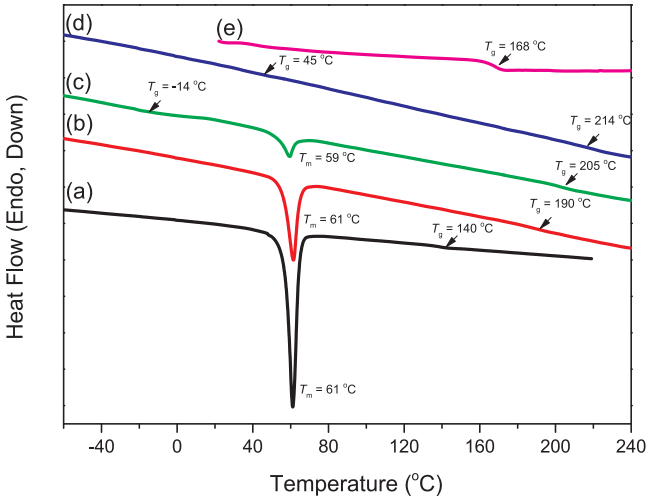

Fig. 1. DSC traces (second heating scans) of various PMMA-*b*-PVPh/P4VP-*b*-PEO blends: (a) 0/100, (b) 30/70, (c) 50/50, (d) 70/30, and (e) 100/0.

Fig. 1 displays second-run thermograms, from −60 to +240 °C, of PMMA-*b*-PVPh/P4VP-*b*-PEO blends of various compositions. The pure P4VP-*b*-PEO diblock copolymer exhibited a glass transition temperature (T_g) of 140 °C for the P4VP block and the melting temperature (T_m) of 61 °C for PEO block [Fig. 1(a)]; we could not observe the value of T_g for the PEO block due to the high crystallinity of the P4VP-*b*-PEO copolymer. The thermogram for the PMMA-*b*-PVPh copolymer exhibited only a single T_g (at 168 °C), suggesting that the PVPh/PMMA pair was miscible through hydrogen bonding. The enthalpy and temperature of melting for the PEO block segment both decreased upon increasing the concentration of PMMA-*b*-PVPh, owing to hydrogen bonding between the PVPh/PEO blocks and dipole–dipole interactions in the PMMA/PEO miscible phase. The thermogram of the PMMA-*b*-PVPh/P4VP-*b*-PEO = 70/30 sample did not display the melting temperature for the PEO segment; instead, it featured only two T_g values at 214 and 45 °C. The higher value presumably corresponded to the miscible PVPh/P4VP domain, featuring strong hydrogen bonding; this value of T_g is significantly higher than those of all of the individual block segments used in this study. The lower value of T_g presumably represented the miscible PMMA/PEO domain. As a result, we suspected that two microphase-separated amorphous phases—namely miscible PVPh/P4VP and PMMA/PEO binary domains—existed at this composition. Furthermore, the higher of the two T_g values, corresponding to the miscible PVPh/P4VP phase, decreased upon increasing the content of P4VP-*b*-PEO, but the resulting glass transition temperatures remained higher than those of PVPh/P4VP = 50/50 homopolymer blends formed from DMF solution (T_g = 190 °C) [53]; thus, it appeared that the microphase

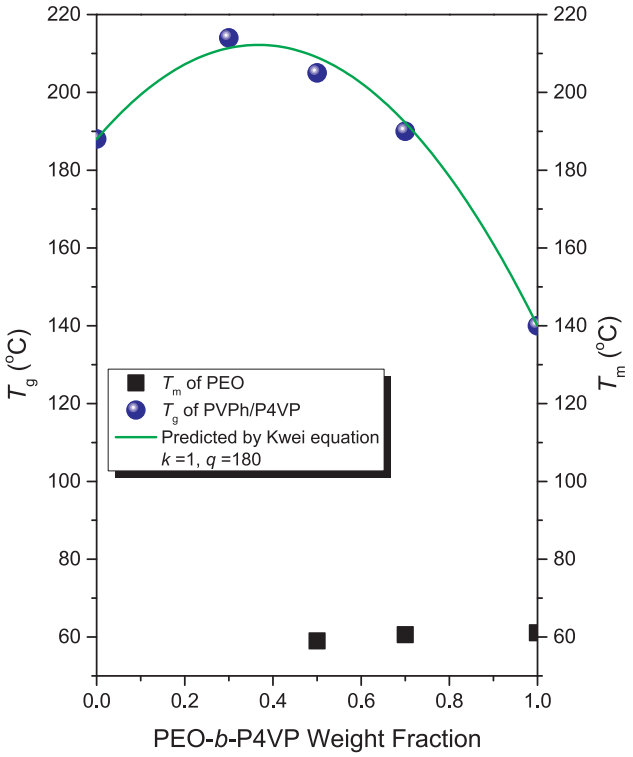

Fig. 2. Values of T_m of the PEO segment and T_g of the miscible PVPh/P4VP domain, as predicted using the Kwei equation, for various PMMA-*b*-PVPh/P4VP-*b*-PEO blends.

separation in the diblock copolymer mixture could occur with a nanoconfinement effect that, subsequently, induce the higher observed values of T_g.

Fig. 2 summarizes the values of T_m of the PEO segment and the values of T_g of the miscible PVPh/P4VP domains in the PMMA-*b*-PVPh/P4VP-*b*-PEO blends. The value of T_m of the PEO segment decreased slightly with the increase of PMMA-*b*-PVPh content; the T_g value of the miscible PVPh/P4VP domain exhibited a positive deviation from that expected from the linear rule. For strongly hydrogen bonding polymer pairs, the values of T_g can be predicted using the Kwei equation [58]

$$T_g = \frac{W_1 T_{g1} + kW_2 T_{g2}}{W_1 + kW_2} + qW_1 W_2 \quad (1)$$

where W_i is the weight fraction of the PVPh or P4VP block segment, T_{gi} is the glass transition temperature of the PVPh or P4VP block segment, and the k and q are fitting constant. Using fitting procedures, we obtained the values of k and q of 1 and 180, respectively, suggesting that this system could be classified as one that is strongly hydrogen bonding.

Fig. 3 presents FTIR spectra of various PMMA-*b*-PVPh/P4VP-*b*-PEO blends, measured at room temperature, highlighting the regions of C=O absorption in the PMMA block [Fig. 3(A)], CH_2 wagging in the PEO segment [Fig. 3(B)], and pyridine vibration in the P4VP segment [Fig. 3(C)]. Two absorption peaks appeared at 1730 and 1705 cm^{-1} for the pure PMMA-*b*-PVPh diblock copolymer, corresponding to free and hydrogen-bonded C=O stretching vibrations, respectively [Fig. 3(A)-(e)]. These two absorption peaks could be fitted well by the Gaussian function, as displayed in Fig. 4(A); Table 3 summarizes the fitting results. The fraction of hydrogen-bonded C=O groups in the PMMA segment decreased with the increase of P4VP-*b*-PEO content. As mentioned above, the values of K_A for the various domains in this study followed the order PVPh/P4VP (K_A = 1200) > PVPh/PEO (K_A = 280) > PVPh/PMMA (K_A = 47); thus, the fraction of hydrogen-bonded C=O groups in the PMMA segment decreased with the increase of P4VP-*b*-PEO content [Fig. 3(A)] because the OH groups in the PVPh

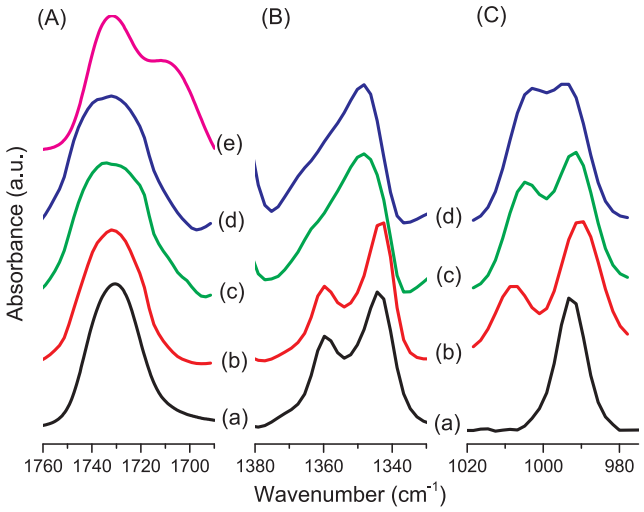

Fig. 3. FTIR spectra of PMMA-*b*-PVPh/P4VP-*b*-PEO blends, displaying the regions of the (A) C=O stretching: (a) pure PMMA, (b) 30/70, (c) 50/50, (d) 70/30, and (e) 100/0. (B) CH_2 wagging, and (C) pyridine vibrations, of various compositions: (a) 0/100, (b) 30/70, (c) 50/50, and (d) 70/30.

segment, which previously interacted with the C=O groups in the PMMA segment of the PMMA-*b*-PVPh diblock copolymer, now interacted with the pyridine units in the P4VP segment, or perhaps the ether units in the PEO segment, after blending with P4VP-*b*-PEO.

Fig. 3(B) displays the FTIR spectral region for CH_2 wagging of the PEO segment. The absorptions at 1360 and 1343 cm^{-1} correspond to the PEO crystalline phase [59]; these two signals were disappeared upon increasing the content of PMMA-*b*-PVPh and, at 50 and 70 wt% of PMMA-*b*-PVPh, was replaced by the broad absorption (near 1350 cm^{-1}) representing the PEO amorphous phase. This result is consistent with the DSC analysis, in which the melting enthalpy of the PEO segment disappeared at 70 wt% of PMMA-*b*-PVPh. We obtained a similar result from the WAXD analyses in Fig. 5(A). Two strong $(0\,3\,2)_{PEO}$ and $(1\,2\,0)_{PEO}$ diffraction peaks appeared for pure P4VP-*b*-PEO, but they disappeared when the sample contained 70 wt% of PMMA-*b*-PVPh. These two peaks also disappeared for the PMMA-*b*-PVPh/P4VP-*b*-PEO = 30/70 blend when the temperature was 80 or 150 °C [Fig. 5(B)]; these temperatures are higher than the melting temperature of the PEO segment (T_m = 61 °C) [60]. Fig. 3(C) presents the FTIR spectral region for the pyridine units for P4VP segment. For pure P4VP-*b*-PEO, the signal for the free pyridyl ring appeared at 993 cm^{-1}; a new band, corresponding to the hydrogen-bonded pyridine units, appeared at 1005 cm^{-1} after blending with PMMA-*b*-PVPh. After fitting these two absorption peaks to Gaussian functions, we observed [Fig. 4(B), Table 3] that the fraction of hydrogen-bonded pyridine units increased with the increase of PMMA-*b*-PVPh content, as expected.

3.2. Self-assembled nanostructures in PMMA-b-PVPh/P4VP-b-PEO blends

Fig. 6(a) reveals that the SAXS pattern of pure P4VP-*b*-PEO did not feature any peaks, implying that a miscible disordered structure existed at lower temperature [61]. Similarly, the SAXS pattern of pure PMMA-*b*-PVPh also exhibited no peaks [Fig. 6(e)], also suggesting that a miscible disordered structure formed, in this case because of the hydrogen bonding interactions. In contrast, all of the SAXS patterns of the PMMA-*b*-PVPh/P4VP-*b*-PEO blends featured scattering peaks, indicating that self-assembled structures formed in this diblock copolymer mixture. We used TEM to investigate these self-assembled structures (Fig. 7). For PMMA-*b*-PVPh/P4VP-*b*-PEO = 30/70, the SAXS pattern provided evidence for only short range order, with one broad peak [Fig. 7(a)], suggesting a wormlike micelle structure—as confirmed in the TEM images in Fig. 7(b) and (c). The *d*-spacing of 21.8 nm, extracted from

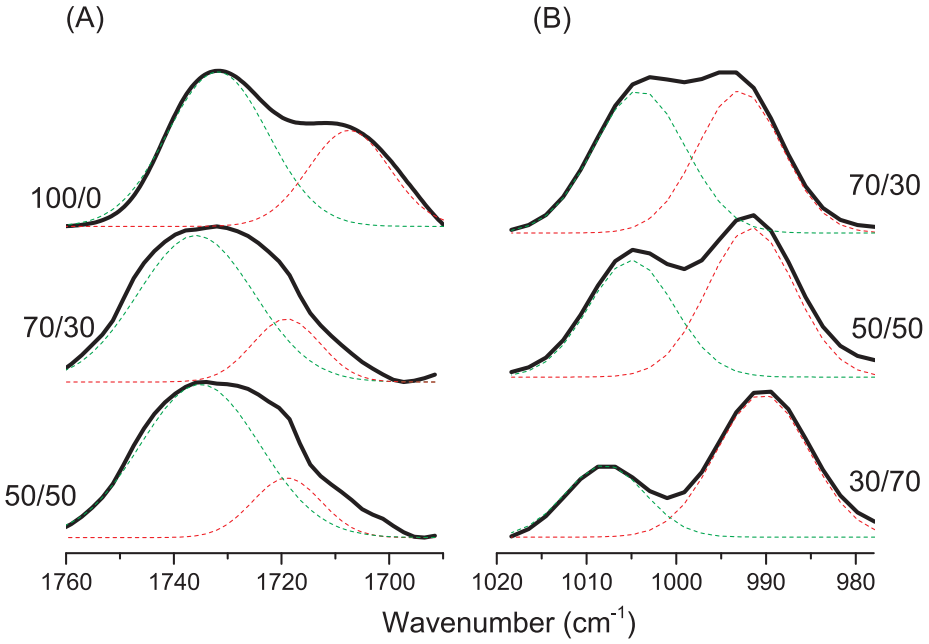

Fig. 4. Curve fitting of the FTIR spectral data for the (A) C═O stretching and (B) pyridine vibrations of PMMA-*b*-PVPh/P4VP-*b*-PEO blends of various compositions.

Table 3
FTIR spectroscopic data for PMMA-*b*-PVPh/P4VP-*b*-PEO diblock copolymer mixtures.

PVPh-*b*-PMMA/PEO-*b*-P4VP	Fee C═O		H-bonded C═O		$f_b^{C=O}$	FreePyridine		H-BondedPyridine		$f_b^{pyridine}$
	v, cm^{-1}	A_f (%)	*v*, cm^{-1}	A_f (%)		*v*, cm^{-1}	A_f (%)	*v*, cm^{-1}	A_f (%)	
100/0	1731	66.7	1707	33.3	0.249	–	–	–	–	–
70/30	1735	79.7	1719	20.3	0.144	993	48.0	1005	51.9	0.519
50/50	1735	81.6	1719	18.4	0.130	992	56.4	1005	43.6	0.436
30/70	1735	100	–	–	0	993	69.5	1007	30.5	0.305
0/100	–	–	–	–		993	100	–	–	0

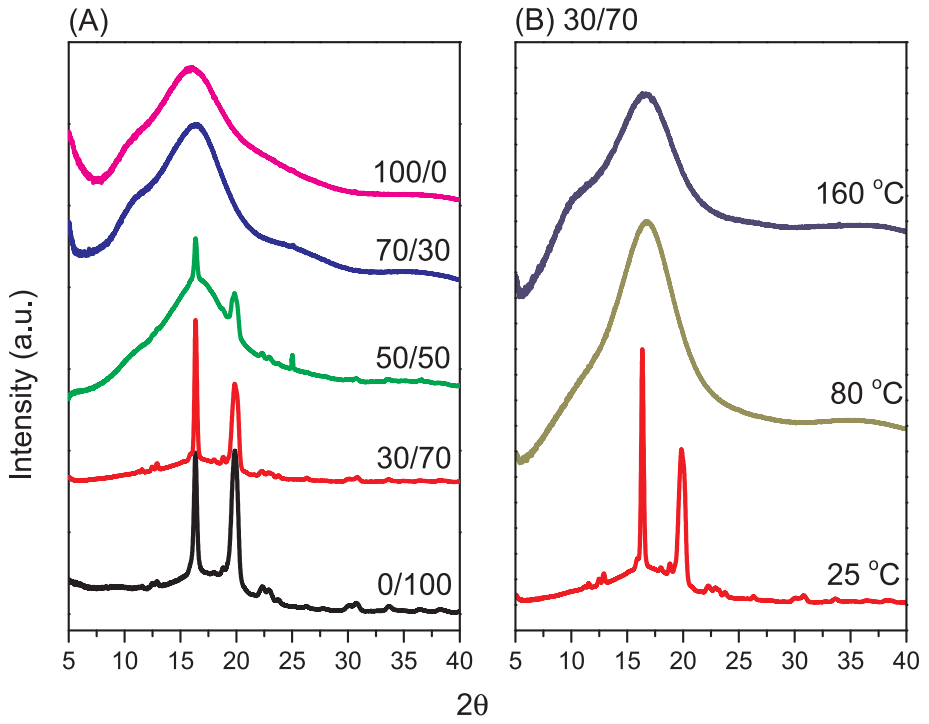

Fig. 5. WAXD analyses of PMMA-*b*-PVPh/P4VP-*b*-PEO blends: (A) various compositions at room temperature; (B) various temperatures for the 30/70 composition.

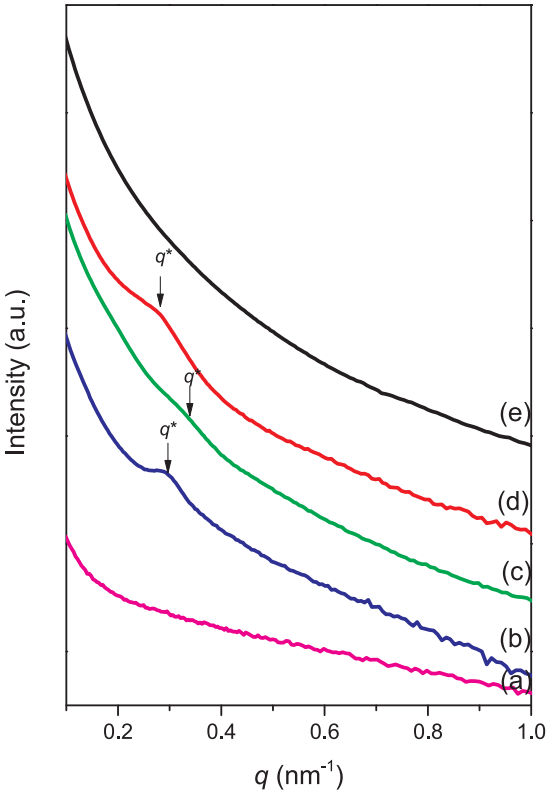

Fig. 6. SAXS patterns, recorded at room temperature, of various PMMA-*b*-PVPh/P4VP-*b*-PEO blends: (a) 0/100, (b) 30/70, (c) 50/50, (d) 70/30, and (e) 100/0.

the first scattering peak at a value of q^* of 0.288 nm^{-1}, was consistent with the spherical size based on the TEM images. Upon increasing the content of PMMA-*b*-PVPh to 50 or 70 wt%, the SAXS patterns also displayed only a single peak [Fig. 7(d) and (g)], but the long-range order of lamellar structures was evident in the corresponding TEM images [Fig. 7(e) and (f) and Fig. 7(h) and (i), respectively]. The *d*-spacings in these lamellar structures were 19.5 nm (q^* = 0.322 nm^{-1}) for PMMA-*b*-PVPh/P4VP-*b*-PEO = 50/50 and 22.2 nm (q^* = 0.283 nm^{-1}) for PMMA-*b*-PVPh/P4VP-*b*-PEO = 70/30. The *d*-spacings of these lamellar structures were also consistent with the lamellar sizes determined from the TEM images. The intensity of a signal in a SAXS pattern should correlate with the electron density difference between the two phases; our system, however, may have featured six different electron density pairs—similar to the depiction in Scheme 4 with six different interaction parameters. As a result, it is possible that the *q* reflections were not easy to detect in our blends, because of the complicated mixture of electron density differences, as we have also noted in previous studies [50]. Scheme 1(C) presents a possible structure for the self-assembly lamellae. Fig. 8 displays the effect of fraction of hydrogen bonded interaction of the functional groups on the morphology based on FTIR and TEM results. Clearly, at relative lower P4VP-*b*-PEO concentration (30 and 50 wt%), which both exhibit the much better ordered lamellar structure, compared with 70 wt% of P4VP-*b*-PEO concentration with the lowest fraction of hydrogen bonded C = O and pyridine units, which exhibit the worm-like structure. In this PMMA-*b*-PVPh/P4VP-*b*-PEO blend system, the fraction of hydrogen bonded functional units actually strongly affect the self-assembly structures; however, the composition effect may also play the important role in this study.

4. Conclusions

We have prepared two miscible disorder diblock copolymers,

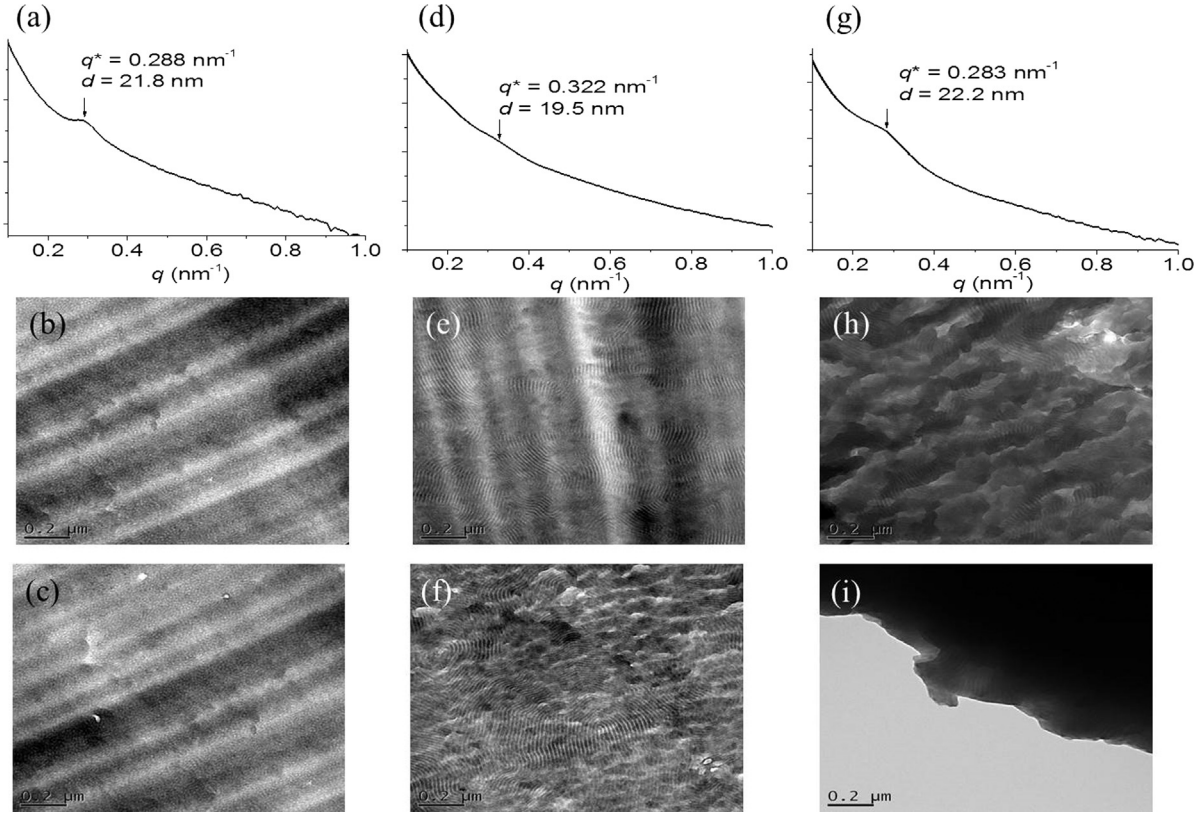

Fig. 7. SAXS patterns and TEM images (after staining with I_2) of various PMMA-*b*-PVPh/P4VP-*b*-PEO blends, recorded at room temperature: (a–c) 30/70, (d–f) 50/50, and (g–i) 70/30.

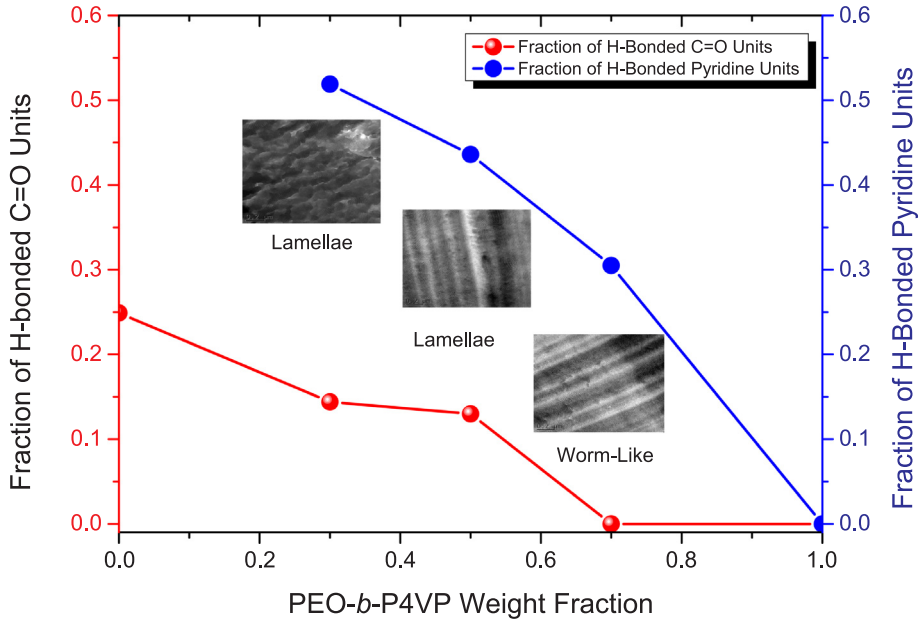

Fig. 8. The effect of fraction of hydrogen bonded interaction of the functional groups on the morphology based on FTIR and TEM results.

PMMA-*b*-PVPh and P4VP-*b*-PEO, through anionic and RAFT polymerizations, respectively. Based on FTIR spectral analyses, the fraction of hydrogen-bonded C═O groups in the PMMA segment of PMMA-*b*-PVPh decreased upon increasing the content of P4VP-*b*-PEO, as expected because the values of K_A followed the order PVPh/P4VP (K_A = 1200) > PVPh/PEO (K_A = 280) > PVPh/PMMA (K_A = 47.1), suggesting that the PVPh block would prefer to hydrogen bond with P4VP and PEO blocks, rather than with the PMMA block. Nevertheless, the PMMA segment exhibited miscibility with the PEO segment. Thus, mixtures of the PMMA-*b*-PVPh/P4VP-*b*-PEO diblock copolymer could exhibit two-phase behavior: we observed the self-assembly of both wormlike and lamellar structures. We believe that this paper is the first to describe two miscible disordered diblock copolymers, when mixed and taking advantage of the Δ*K* effect with different hydrogen bonding interactions, forming a self-assembled nanostructure.

Acknowledgment

This study was supported financially by the Ministry of Science and Technology, Taiwan, under contracts MOST 106-2221-E-110-067-MY3 and 105-2221-E-110-092-MY3.

Appendix A. Supplementary material

Supplementary data to this article can be found online at https://doi.org/10.1016/j.eurpolymj.2019.04.037.

References

[1] S.W. Kuo, Hydrogen Bonding in Polymeric Materials, John Wiley & Sons, Hoboken, NJ, USA, 2018.
[2] R. Bahrami, T.I. Lobling, H. Schmalz, A.H.E. Muller, V. Altstadt, Synergistic effects of Janus particles and triblock terpolymers on toughness of immiscible polymer blends, Polymer 109 (2017) 229–237.
[3] Y. Zhao, X. Zhao, M. Roders, A. Gumyusenge, A.L. Ayzner, J. Mei, Melt-Processing of complementary semiconducting polymer blends for high performance organic transistors, Adv. Mater. 29 (2017) 1605056.
[4] X. Wang, S. Huang, Y. Wang, P. Wei, Y. Chen, Eco-friendly cellulose acetate butyrate/poly(butylene succinate) blends: crystallization, miscibility, thermostability, rheological and mechanical properties, J. Polym. Res. 24 (2017) 16.
[5] Y.C. Lin, Y.W. Su, J.X. Li, B.H. Lin, C.H. Chen, H.C. Chen, K.H. Wu, Y. Yang, K.H. Wei, Energy transfer within small molecule/conjugated polymer blends enhances photovoltaic efficiency, J. Mater. Chem. A 5 (2017) 18053–18063.
[6] K.E. Feldman, M.J. Kade, T.F.A. de Greel, E.W. Meijer, E.J. Kramer, C.J. Hawker, Polymers with multiple hydrogen-bonded end groups and their blends, Macromolecules 41 (2008) 4694–4700.
[7] K.E. Feldman, M.J. Kade, E.W. Meijer, C.J. Hawker, E.J. Kramer, Phase behavior of complementary multiply hydrogen bonded end-functional polymer blends, Macromolecules 43 (2010) 5121–5127.
[8] J. Rao, E. Paunescu, M. Mirmohades, I. Gadwal, C.J. Hawker, J. Bang, A. Khan, Supramolecular mimics of phase separating covalent diblock copolymers, Polym. Chem. 3 (2012) 2050–2056.
[9] S.K. Yang, A.V. Ambade, M. Weck, Main-chain supramolecular block copolymers, Chem. Soc. Rev. 40 (2011) 129–137.
[10] J.F. Gohy, B.G.G. Lohmeijer, U.S. Schubert, Metallo-supramolecular block copolymer micelles, Macromolecules 35 (2002) 4560–4563.
[11] S.A. Jenekhe, X.L. Chen, Self-assembly of ordered microporous materials from rod-coil block copolymers, Science 283 (1999) 372–375.
[12] A.R. Guiod, W.M. Vandermeulen, V.H. Klok, Advanced drug delivery devices via self-assembly of amphiphilic block copolymers, Adv. Drug Deliv. Rev. 64 (2012) 270–279.
[13] E.L. Lin, W.L. Hsu, Y.W. Chiang, Trapping structural coloration by a bioinspired gyroid microstructure in solid state, ACS Nano 12 (2018) 485–493.
[14] C.C. Tsai, Z. Gan, S.W. Kuo, Using benzoxazine chemistry and bio-based triblock copolymer to prepare functional porous polypeptide capable of efficient dye adsorption, Polym. Chem. 9 (2018) 3684–3693.
[15] J. Tang, J. Liu, C. Li, Y. Li, M.O. Tade, S. Dai, Y. Yamauchi, Synthesis of nitrogen-doped mesoporous carbon spheres with extra-large pores through assembly of diblock copolymer micelles, Angew. Chem. Int. Ed. 54 (2015) 588–593.
[16] Y.T. Shieh, P.Y. Lin, S.W. Kuo, Sequence length distribution affects the lower critical solution temperature, glass transition temperature, and CO2-responsiveness of N-isopropylacrylamide/methacrylic acid copolymers, Polymer 143 (2018) 258–270.
[17] C.Y. Yu, S.W. Kuo, Phenolic functionality of polyhedral oligomeric silsesquioxane nanoparticles affects self-assembly supramolecular structures of block copolymer hybrid complexes, Ind. Eng. Chem. Res. 57 (2018) 2546–2559.
[18] Y.K. Han, E.M. Pearce, T.K. Kwei, Poly(styrene-b-vinylphenyldimethylsilanol) and its blends with homopolymers, Macromolecules 33 (2000) 1321–1329.
[19] J.Q. Zhao, E.M. Pearce, T.K. Kwei, Binary and ternary blends of polystyrene-block-poly(p-hydroxystyrene), Macromolecules 30 (1997) 7119–7126.
[20] K. Dobrosielska, S. Wakao, A. Takano, Y. Matsushita, Nanophase-separated structures of AB block copolymer/C homopolymer blends with complementary hydrogen-bonding interactions, Macromolecules 41 (2008) 7695–7698.
[21] K. Dobrosielska, S. Wakao, J. Suzuki, K. Noda, A. Takano, Y. Matsushita, Effect of homopolymer molecular weight on nanophase-separated structures of AB block copolymer/C homopolymer blends with hydrogen-bonding interactions, Macromolecules 42 (2009) 7098–7102.
[22] S.C. Chen, S.W. Kuo, U.S. Jeng, C.J. Su, F.C. Chang, On modulating the phase behavior of block copolymer/homopolymer blends via hydrogen bonding, Macromolecules 43 (2010) 1083–1092.
[23] A. Dehghan, A.C. Shi, Modeling hydrogen bonding in diblock copolymer/homopolymer blends, Macromolecules 46 (2013) 5796–5805.
[24] S.C. Tsai, Y.C. Lin, E.L. Lin, Y.W. Chiang, S.W. Kuo, Hydrogen bonding strength effect on self-assembly supramolecular structures of diblock copolymer/homopolymer blends, Polym. Chem. 7 (2016) 2395–2409.
[25] N. Hameed, Q. Guo, Nanostructure and hydrogen bonding in interpolyelectrolyte complexes of poly(ε-caprolactone)-block-poly(2-vinyl pyridine) and poly(acrylic acid), Polymer 49 (2008) 5268–5275.

[26] N. Hameed, J. Liu, Q. Guo, Self-assembled complexes of poly(4-vinylphenol) and poly(ε-caprolactone)-block-poly (2-vinylpyridine) via competitive hydrogen bonding, Macromolecules 41 (2008) 7596–7605.
[27] N. Hameed, Q. Guo, Selective hydrogen bonding and hierarchical nanostructures in poly(hydroxyether of bisphenol A)/poly(ε-caprolactone)-block-poly(2-vinyl pyridine) blends, Polymer 49 (2008) 922–933.
[28] W.C. Chen, S.W. Kuo, C.H. Lu, U.S. Jeng, F.C. Chang, Self-assembly structures through competitive interactions of crystalline – amorphous diblock copolymer/homopolymer blends: poly(ε-caprolactone-b-4-vinyl pyridine)/poly(vinyl phenol), Macromolecules 42 (2009) 3580–3590.
[29] N.V. Salim, T. Hanley, Q. Guo, Microphase separation through competitive hydrogen bonding in double crystalline diblock copolymer/homopolymer blends, Macromolecules 43 (2010) 7695–7704.
[30] J.G. Li, Y.D. Lin, S.W. Kuo, From microphase separation to self-organized mesoporous phenolic resin through competitive hydrogen bonding with double-crystalline diblock copolymers of poly(ethylene oxide-b-ε-caprolactone), Macromolecules 44 (2011) 9295–9309.
[31] N.V. Salim, N. Hameed, Q. Guo, Competitive hydrogen bonding and self-assembly in poly(2-vinyl pyridine)-block-poly(methyl methacrylate)/poly(hydroxyether of bisphenol A) blends, J. Polym. Sci. Part B: Polym. Phys. 47 (2009) 1894–1905.
[32] N. Hameed, N.V. Salim, Q. Guo, Microphase separation through competitive hydrogen bonding in self-assembled diblock copolymer/homopolymer complexes, J. Chem. Phys. 131 (2009).
[33] H.F. Lee, S.W. Kuo, C.F. Huang, J.S. Lu, S.C. Chan, C.F. Wang, F.C. Chang, Hydrogen-bonding interactions mediate the phase behavior of an AB/C block copolymer/homopolymer blend comprising poly methyl methacrylate-b-vinylpyrrolidone) and poly (vinylphenol), Macromolecules 39 (2006) 5458–5465.
[34] W.C. Chen, S.W. Kuo, U.S. Jeng, F.C. Chang, Self-assembly through competitive interactions of miscible diblock copolymer/homopolymer blends: Poly (vinylphenol-b-methyl methacrylate)/poly (vinylpyrrolidone) blend, Macromolecules 41 (2008) 1401–1410.
[35] J. Zhou, A.C. Shi, Microphase separation induced by differential interactions in diblock copolymer/homopolymer blends, J. Chem. Phys. 130 (2009).
[36] I. Lin, S.W. Kuo, F.C. Chang, Self-assembly structures through competitive interactions of miscible crystalline–amorphous diblock copolymer/homopolymer blends, Polymer 40 (2009) 5276–5287.
[37] C.C. Tsai, Z. Gan, T. Chen, S.W. Kuo, Competitive hydrogen bonding interactions influence the secondary and hierarchical self-assembled structures of polypeptide-based triblock copolymers, Macromolecules 51 (2018) 3017–3029.
[38] W.C. Su, Y.S. Wu, C.F. Wang, S.W. Kuo, Self-assembled structures of diblock copolymer/homopolymer blends through multiple complementary hydrogen bonds, Crystals 8 (2018) 330.
[39] C.F. Huang, W.H. Chen, J. Aimi, S. Huang, S. Venkatesan, Y.W. Chiang, S.H. Huang, S.W. Kuo, T. Chen, Synthesis of well-defined PCL-b-PnBA-b-PMMA ABC-type triblock copolymers: toward the construction of nanostructures in epoxy thermosets, Polym. Chem. 9 (2018) 5644–5654.
[40] Y. Matsushita, Creation of hierarchically ordered nanophase structures in block polymers having various competing interactions, Macromolecules 40 (2007) 771–776.
[41] H. Miyase, Y. Asai, A. Takano, Y. Matsushita, Kaleidoscopic tiling patterns with large unit cells from ABC star-shaped terpolymer/diblock copolymer blends with hydrogen bonding interaction, Macromolecules 50 (2017) 979–986.
[42] T. Asari, S. Matsuo, A. Takano, Y. Matsushita, Three-phase hierarchical structures from AB/CD diblock copolymer blends with complemental hydrogen bonding interaction, Macromolecules 38 (2005) 8811–8815.
[43] T. Asari, S. Arai, A. Takano, Y. Matsushita, Archimedean tiling structures from ABA/CD block copolymer blends having intermolecular association with hydrogen bonding, Macromolecules 39 (2006) 2232–2237.
[44] S.W. Kuo, Hydrogen bond-mediated self-assembly and supramolecular structures of diblock copolymer mixtures, Polym. Inter. 58 (2009) 455–464.
[45] W.C. Chen, S.W. Kuo, F.C. Chang, Self-assembly of an A-B diblock copolymer blended with a C homopolymer and a C–D diblock copolymer through hydrogen bonding interaction, Polymer 51 (2010) 4176–4184.
[46] S.W. Kuo, P.H. Tung, C.L. Lai, K.U. Jeong, F.C. Chang, Supramolecular micellization of diblock copolymer mixtures mediated by hydrogen bonding for the observation of separated coil and chain aggregation in common solvents, Macromol. Rapid Commun. 29 (2008) 229–233.
[47] S.W. Kuo, P.H. Tung, F.C. Chang, Hydrogen bond mediated supramolecular micellization of diblock copolymer mixture in common solvents, Eur. Polym. J. 45 (2009) 1924–1935.
[48] C.H. Hsu, S.W. Kuo, J.K. Chen, F.H. Ko, C.S. Liao, F.C. Chang, Self-assembly behavior of AB diblock and CD random copolymer mixtures in the solution state through mediated hydrogen bonding, Langmuir 24 (2008) 7727–7734.
[49] C. Tang, E.M. Lennon, G.H. Fredrickson, E.J. Kramer, C.J. Hawker, Evolution of block copolymer lithography to highly ordered square arrays, Science 322 (2008) 429–432.
[50] T.C. Tseng, S.W. Kuo, Hydrogen-bonding strength influences hierarchical self-assembled structures in unusual miscible/immiscible diblock copolymer blends, Macromolecules 51 (2018) 6451–6459.
[51] T.C. Tseng, S.W. Kuo, Hierarchical self-assembled structures from diblock copolymer mixtures by competitive hydrogen bonding strength, Molecules 23 (2018) 2242.
[52] C.L. Lin, W.C. Chen, C.S. Liao, Y.C. Su, C.F. Huang, S.W. Kuo, F.C. Chang, Sequence distribution and polydispersity index affect the hydrogen-bonding strength of poly (vinylphenol-co-methyl methacrylate) copolymers, Macromolecules 38 (2005) 6435–6444.
[53] S.W. Kuo, P.H. Tung, F.C. Chang, Syntheses and the study of strongly hydrogen-bonded poly (vinylphenol-b-vinylpyridine) diblock copolymer through anionic polymerization, Macromolecules 39 (2006) 9388–9395.
[54] M.M. Coleman, P.C. Painter, Miscible Polymer Blends: Background and Guide for Calculations and Design, DEStech Publication Inc., Lancaster, PA, 2006.
[55] J.A. Zawada, C.M. Ylitalo, G.G. Fuller, R.H. Colby, T.E. Long, Component relaxation dynamics in a miscible polymer blend: poly(ethylene oxide)/poly(methyl methacrylate), Macromolecules 25 (1992) 2896–2902.
[56] N. Parizel, F. Laupretre, L. Monnerie, N.m.r. and d.s.c. investigations of the miscibility of poly(methyl methacrylate)/poly(ethylene oxide) blends, Polymer 38 (1997) 3719–3725.
[57] S.W. Kuo, W.J. Huang, C.F. Huang, S.C. Chan, F.C. Chang, Miscibility, specific interactions, and spherulite growth rates of binary poly (acetoxystyrene)/poly (ethylene oxide) blends, Macromolecules 37 (2004) 4164–4173.
[58] T. Kwei, The effect of hydrogen bonding on the glass transition temperatures of polymer mixtures, J. Polym. Sci. Polym. Lett. Ed. 22 (1984) 307–313.
[59] S.W. Kuo, C.L. Lin, F.C. Chang, Phase behavior and hydrogen bonding in ternary polymer blends of phenolic resin/poly ethylene oxide)/poly (ε-caprolactone), Macromolecules 35 (2002) 278–285.
[60] Y.W. Chiang, Y.Y. Hu, J.N. Li, S.H. Huang, S.W. Kuo, Trilayered single crystals with epitaxial growth in poly (ethylene oxide)-block-poly (ε-caprolactone)-block-poly (l-lactide) thin films, Macromolecules 48 (2015) 8526–8533.
[61] C.L. Yeh, T. Hou, H.L. Chen, L.Y. Yeh, F.C. Chiu, A.J. Muller, N. Hadjichristidis, Lower critical ordering transition of poly(ethyleneoxide)-block-poly(2-vinylpyridine), Macromolecules 44 (2011) 440–443.